Ballistic transport and quantum interference in InSb nanowire devices*

Sen Li(李森)[1], Guang-Yao Huang(黄光耀)[1], Jing-Kun Guo(郭景琨)[1], Ning Kang(康宁)[1,†], Philippe Caroff[2,3], and Hong-Qi Xu(徐洪起)[1,‡]

[1] *Key Laboratory for the Physics and Chemistry of Nanodevices and Department of Electronics, Peking University, Beijing* 100871, *China*
[2] *Department of Electronic Materials Engineering, Research School of Physics and Engineering, The Australian National University, Canberra, ACT* 0200, *Australia*
[3] *Institute of Electronics Microelectronics and Nanotechnology, CNRS-UMR* 8520, *Avenue Poincaré, C. S.* 60069, 59652 *Villeneuve d'Ascq, France*

(Received 13 December 2016; revised manuscript received 19 December 2016; published online 10 January 2017)

An experimental realization of a ballistic superconductor proximitized semiconductor nanowire device is a necessary step towards engineering topological quantum electronics. Here, we report on ballistic transport in InSb nanowires grown by molecular-beam epitaxy contacted by superconductor electrodes. At an elevated temperature, clear conductance plateaus are observed at zero magnetic field and in agreement with calculations based on the Landauer formula. At lower temperature, we have observed characteristic Fabry–Pérot patterns which confirm the ballistic nature of charge transport. Furthermore, the magnetoconductance measurements in the ballistic regime reveal a periodic variation related to the Fabry–Pérot oscillations. The result can be reasonably explained by taking into account the impact of magnetic field on the phase of ballistic electron's wave function, which is further verified by our simulation. Our results pave the way for better understanding of the quantum interference effects on the transport properties of InSb nanowires in the ballistic regime as well as developing of novel device for topological quantum computations.

Keywords: InSb nanowire, ballistic transport,quantum interference

PACS: 73.23.–b, 73.23.Ad, 73.63.–b, 73.63.Nm **DOI:** 10.1088/1674-1056/26/2/027305

1. Introduction

Semiconductor nanowires are appealing candidates for constructing novel devices in nanoelectronics.[1] Among them, InSb nanowires have been investigated for applications in high-speed electronics,[2] spintronics,[3] and quantum computing,[4,5] due to their remarkable properties such as a high electron mobility, a strong spin–orbit coupling,[6] and a large Landé g-factor,[7–9] Recently, it has been theoretically proposed[10,11] and experimentally realized[12,13] that hybrid devices based on these nanowires can be made as hosts for Majorana bound states (MBS) in solid state. Beside the essential ingredients such as proximity induced superconductivity and strong spin-orbit coupling, the ballistic transport inside the nanowire with the tunability of one-dimensional (1D) modes is also a key requisite and is seldom explored. For ballistic transport in 1D systems, quantized conductance plateaus emerge as a result of the 1D subband spectrum and have been routinely observed in constrictions formed in two-dimensional electron gas (2DEG).[14,15] Besides, the coherent electron waves traveling inside a ballistic channel can have interference effect, leading to a Fabry–Pérot pattern in the conductance spectroscopy. Such patterns have been well observed and used as siganatures of ballistic transport in carbon nanotubes[16,17] and in III–V nanowires.[18–20] Very recently, quantized conductance in InSb nanowires at zero magnetic field has been demonstrated with normal metal contacts.[21] However, an extensive and direct demonstration on the ballistic nature of superconductor contacted nanowire device remains challenging and largely unexplored.

Here, we report on the ballistic transport behavior in InSb nanowires with superconductor contacts. In this work, we focus on measurements of the devices in the normal state either at a high temperature ($> T_c$) or with a small magnetic field ($> B_c$) applied. We observe well defined conductance plateaus in the InSb nanowire device at an elevated temperature, which is a direct signature of ballistic transport in the nanowire and can be well described by the Landauer approach. Through analysis of consistent fitting, a mean free path $l_e \approx 90$ nm is extracted. At lower temperature, conductance oscillations as a result of the Fabry–Pérot interference are observed and characterized with bias spectroscopy. We further measure the low temperature magnetoconductance patterns in Fabry–Pérot regime. The evolution of magnetoconductance as a function of gate voltage can be attributed to the quantum interference effects in such a ballistic system. Previous magnetotransport measure-

*Project supported by the National Key Basic Research and Development Project of the Ministry of Science and Technology of China (Grant No. 2016YFA0300601) and the National Natural Science Foundation of China (Grant Nos. 91221202, 91421303, 11374019, and 61321001).

†Corresponding author. E-mail: nkang@pku.edu.cn
‡Corresponding author. E-mail: hqxu@pku.edu.cn

© 2017 Chinese Physical Society and IOP Publishing Ltd

ments have been utilized in nanowires to study phase coherent processes and extract various mesoscopic length scales.[22–24] However, most of them have been carried out in the diffusive regime with few efforts on the (quasi) ballistic regime.[25,26] Our result can be well understood by considering a phase shift induced by the magnetic field, which reveals the quantum interference nature of the transport process.

2. Experiment

InSb nanowires investigated in this study are grown by gold catalyzed gas-source molecular beam epitaxy on InP(111)B substrate following the growth of a stem segment of InAs.[9] The InSb nanowires have diameters of 50 nm–80 nm and lengths up to 3 μm, exhibiting a pure zinc blende crystal structure, free from twin defects and tapering.[27,28] After growth, the InSb nanowires are mechanically transferred onto an n^{++}-doped Si substrate with an 110-nm thick thermally oxided top layer used as a global back gate. Ti/Al (5 nm/90 nm) contacts are patterned on the located individual InSb nanowires by standard electron beam lithography, followed by e-beam evaporation and lift-off processes. Before contact deposition, the nanowires are treated with a brief sulfur passivation process to remove the surface oxide and meliorate the contact interface. The superconducting contacts have been characterized in our previous work to have a critical temperature $T_c \sim 1$ K and a critical field $B_c \sim 25$ mT.[19] The devices studied in this work have contact separations of 60 nm–100 nm and diameters of 60 ± 5 nm. A typical scanning electron microscope image of devices investigated in this work is shown in Fig. 1(a). The samples are mounted into a dilution refrigerator and measured with both dc and ac techniques. Electronic transport measurements are carried out at refrigerator temperatures between 10 mK and 10 K. The external magnetic field is applied perpendicular to the substrate plane.

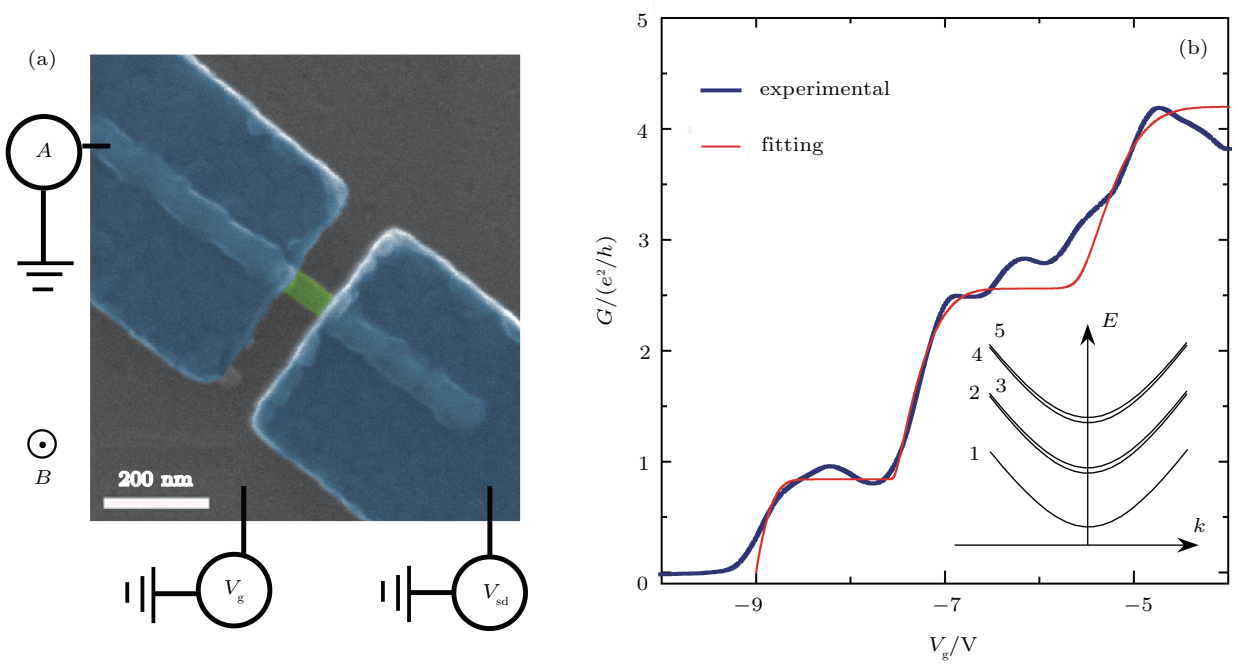


Fig. 1. (color online) (a) False-color SEM image of a typical InSb nanowire device. The InSb nanowire (green) of typical diameter 60 ± 5 nm is contacted by two Ti/Al (5 nm/90 nm) superconducting electrodes. The contact spacings are in a range of 60 nm–100 nm. (b) Differential conductance G as a function of back gate voltage V_g measured at $T = 10$ K and $B = 0$ T using an ac bias $V_{ac} = 100$ μeV (blue curve). Red curve is a fit to the experimental data based on the Landauer formula of conductance. Inset: schematic of the 1D subbands of an InSb nanowire. The second and third as well as the fourth and fifth subband are nearly degenerate owing to an additional symmetry of the nanowire discussed in the main text.

3. Results and discussion

We first show the results of a device with a nanowire diameter $d \sim 60$ nm and a contact spacing $L \sim 70$ nm. The conductance G as a function of the back gate voltage V_g measured by ac method at a temperature of 10 K and zero magnetic field is plotted in Fig. 1(b) (blue curve). As can be clearly seen, well-resolved plateaus develop in the $G(V_g)$ trace at $\sim 1.0\ e^2/h$, $2.6\ e^2/h$, and $4.0\ e^2/h$. Similar features have also been observed in a different nanowire device. With the aid of the finite bias and the magnetic field evolution of the differential conductance, it is corroborated that the observed plateau feature is a result of the ballistic transport through the 1D subbands of the nanowires. The larger heights of the second and third plateau result from the additional degeneracies of the subbands, since the second and third subband as well as the fourth and fifth subband are (nearly) degenerate owing to the rotational symmetry of the nanowire[21,29] (see inset of Fig. 1(b)). As a result, the conductance is supposed to develop plateaus at $2\ e^2/h$, $6\ e^2/h$, and $10\ e^2/h$ as the degenerate subbands are populated, instead of at $2\ e^2/h$, $4\ e^2/h$, and $6\ e^2/h$.

Obviously, there are discrepancies between the experimental plateau values and the ideal ones. We attribute this to the finite transparencies of the contact-nanowire interfaces.[25,30] In order to better understand the experimental results, following the approach introduced earlier by Bagwell *et al.*,[31] we perform simulation with the use of the generalized Landauer formula including the thermal smearing of the Fermi–Dirac distribution,

$$G = \frac{2e^2}{h}\sum_i \int -T_i(E)\partial f(E)/\partial(E)\,\mathrm{d}E, \tag{1}$$

where $f(E)$ is the Fermi–Dirac distribution. The summation comprises all the degenerate subbands contributing to the transport and $T_i(E)$ is their transmission coefficient. The function between E_F and V_g is established through the relation that the integrated density of states equal to the number of gate voltage-induced carriers per unit length

$$N = \int \rho(E) f(E)\,\mathrm{d}E = C_\mathrm{g}(V_\mathrm{g} - V_\mathrm{T})/e,$$

where C_g is the gating efficiency of the back gate and V_T is the threshold voltage. We use this model to fit our data with C_g, T_i, and the subband spacing $\Delta E_{i,i+1}$ as fitting parameters and the corresponding result is shown as the red curve in Fig. 1(b). As shown in the plot, the experimental data can be well reproduced by the fitting curve, which yields the parameters as $C_\mathrm{g} = 6.5$ pF/m, $\Delta E_{1,2} = 24$ meV, $\Delta E_{3,4} = 17$ meV, $T_1 = 0.42$, $T_2 = 0.43$, and $T_3 = 0.41$. These non unitary transmission coefficients may stem from disorders on the nanowire-contact interface and can well account for the degraded values of the observed plateaus. Using the C_g value above, we obtain a field effect mobility $\mu = 9600\ \mathrm{cm^2/V\cdot s}$ of our nanowires. With an average electron concentration $n \approx 1\times10^{17}\ \mathrm{cm^{-3}}$, the elastic mean free path is estimated to be $l_\mathrm{e} \approx 90$ nm. Therefore, given the fact $L < l_\mathrm{e}$, our result confirms the ballistic transport regime of the device. Meanwhile, this result also indicates that we can accurately control the population of the 1D subbands using a back gate voltage.

Next we turn to another device with a similar nanowire diameter but a longer channel length $L \sim 90$ nm. Here we measured the device at a lower temperature of $T \sim 10$ mK, enabling us to investigate more of the quantum interference effects in the InSb nanowire. Since the Ti/Al contacts become superconducting at such low temperature, we apply a small magnetic field (50 mT) to suppress superconductivity in the Al contacts. The normal state transfer curve $G(V_\mathrm{g})$ is presented in Fig. 2(a). Unlike the plateau shape of the first device at higher temperature in Fig. 1(b), the $G(V_\mathrm{g})$ trace here shows a series of (quasi) periodic oscillations which is also observed in a different device. These oscillations are unlikely to be Coulomb blockade oscillations since they persist over high conductance regions ($\sim 8\ e^2/h$). Since our nanowire devices work in the ballistic transport regime ($L \le l_\mathrm{e}$), electrons through the nanowire experience no scattering except at the nanowire-contact interfaces. Therefore, the universal conductance fluctuations (UCF), which originates from multiple scattering of electrons by randomly distributed disorder, can also be excluded from the transport regime. Hence, the most reasonable explanation to these oscillations is the Fabry–Pérot interference of electron waves, which has been observed and taken as a signature of the ballistic transport in carbon nanotubes[16,17] and semiconductor nanowires.[18–20]

To better characterize the observed quasi-periodic conductance oscillations, we perform transport spectroscopy by measuring the differential conductance $\mathrm{d}I/\mathrm{d}V$ as a function of V_sd and V_g in a typical region of oscillatory conductance (green dashed square in Fig. 2(a)). As shown in Fig. 2(b), the differential conductance in the V_sd–V_g plane shows a clear (partial) checkerboard pattern with quasi-periodic oscillations along both V_sd and V_g. Such a differential conductance pattern is a typical signature of the Fabry–Pérot interference, which can be understood by ballistic charge transport through the resonant states. In a ballistic device, the condition for the constructive Fabry–Pérot interference can be expressed as $k_\mathrm{F} = n\pi/L_\mathrm{c}$, where k_F is the Fermi wavelength, n is an integer and L_c is the Fabry–Pérot cavity length. Since the chemical potential $\mu = \hbar^2 k_\mathrm{F}^2/2m^*$ in the nanowire is proportional to the gate voltage, as the gate voltage is swept, k_F is continuously varied, leading to a periodic satisfaction of the interference condition ($k_\mathrm{F} = n\pi/L_\mathrm{c}$) and thus oscillations in the nanowire conductance. Combining the interference condition with the expression of the electron density of a 1D channel $\delta n = C_\mathrm{g}\Delta V_\mathrm{g}/e = 2\delta k_\mathrm{F}/\pi$, the cavity length can be written as $L_\mathrm{c} = 2e/(C_\mathrm{g}\Delta V_\mathrm{g})$. We apply the fast Fourier transformation (FFT) to the $G(V_\mathrm{g})$ trace in Fig. 2(a) and obtain an average period of the Fabry–Pérot oscillations $\Delta V_\mathrm{g} \sim 0.48$ V. We take the value of C_g as $C_\mathrm{g} = 6.5$ pF/m referring to the result of the first device since the diameters of the nanowires are very close. Accordingly, the cavity length can be calculated as $L_\mathrm{c} = 2e/(C_\mathrm{g}\Delta V_\mathrm{g}) \approx 102$ nm, which is quite consistent with the geometric channel length L of the device. On the other hand, the applied bias voltage eV_sd, which equals to the difference between the chemical potentials of source and drain leads, can also tune the system in or out of constructive Fabry–Pérot interference. The corresponding condition can be written as:

$$eV_\mathrm{sd} = \Delta E_\mathrm{FP} = \hbar^2\delta k_\mathrm{F}^2/2m^* = \pi^2\hbar^2/2m^*L_\mathrm{c}^2,$$

where ΔE_FP is the energy spacing of the virtual resonant states from the constructive Fabry–Pérot interference. From Fig. 2(b), ΔE_FP is estimated to be ~ 2 meV. Hence we can again calculate L_c as $L_\mathrm{c} = \sqrt{\pi^2\hbar^2/2m^2\Delta E_\mathrm{FP}} \approx 110$ nm, which is in good agreement with our previous analysis.

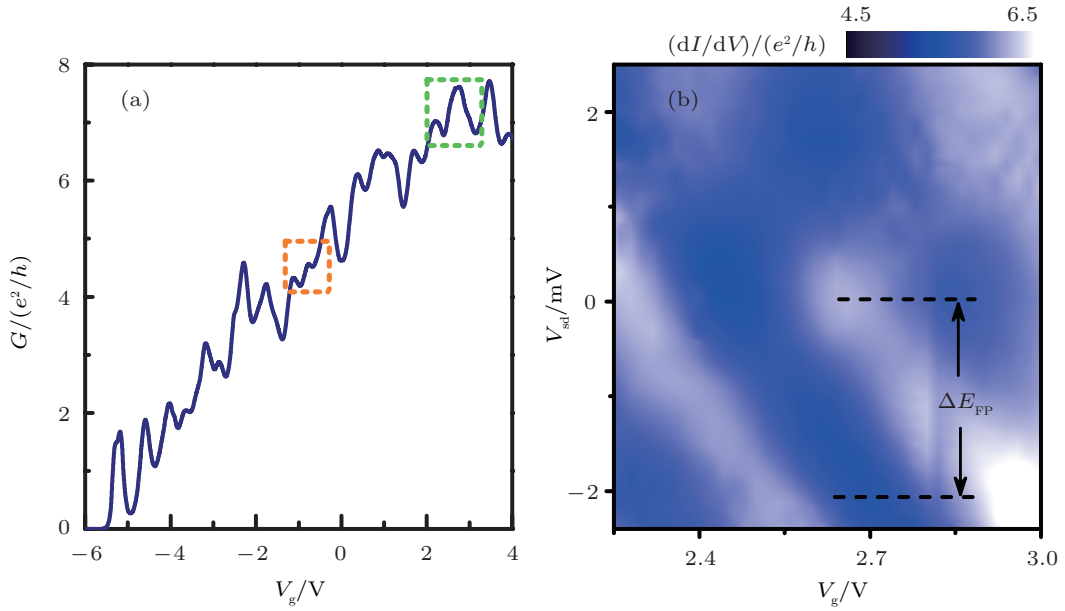


Fig. 2. (color online) (a) Conductance G of a second device as a function of back gate voltage V_g measured at $T = 10$ mK with an ac bias $V_{ac} = 100$ μeV. A small magnetic field $B = 30$ mT is applied to suppress superconductivity in the Al contacts. Green and orange squares mark the regions to be discussed hereinbelow. (b) Differential conductance dI/dV as a function of bias voltage V_{sd} and gate voltage V_g, corresponding to the same range denoted by the green square in panel (a). The nonlinear transport spectroscopy shows a characteristic Fabry–Pérot interference pattern, providing direct experimental evidence for ballistic charge transport through InSb nanowires.

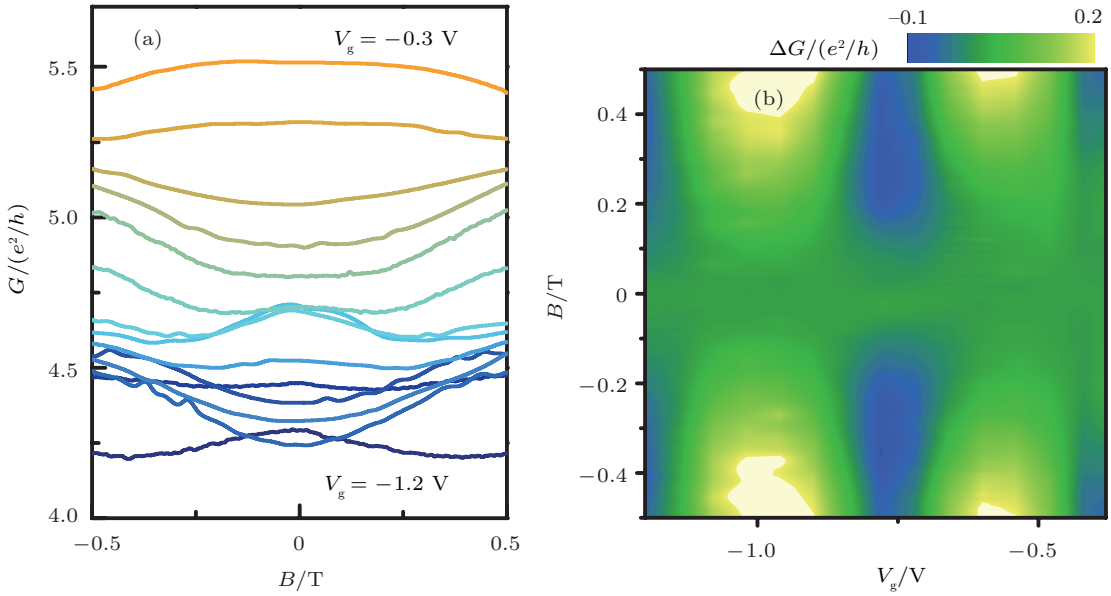


Fig. 3. (color online) (a) Magnetoconductance (MC) traces measured at a temperature of 10 mK from $V_g = -1.2$ V to $V_g = -0.3$ V, corresponding to the same region denoted by the orange square in Fig. 2(a). The step of V_g between adjacent traces is 0.06 V. (b) ΔG as a function of B and V_g obtained by subtracting the conductance at zero magnetic field $G(0)$ from the MC traces. It can be clearly seen that ΔG exhibits a periodic-like behaviour as B and V_g is varied.

Having demonstrated the ballistic transport regime in our device, we move on to study quantum interference effects on the conductance in the presence of a magnetic field. We focus on a region displaying the Fabry–Pérot oscillations (orange dashed square in Fig. 2(a)), and measure the magnetoconductance (MC) in a range of $|B| = 0.5$ T at different V_g. The corresponding data is shown in Fig. 3(a). Strikingly, as V_g is changed, the low field MC curve alters its shape showing either a hump or a valley, which seems to be related with the conductance oscillations at zero magnetic field. The behavior of observed MC might be reminiscent of the appearance of weak localization (WL) or weak anti-localization (WAL) arising from coherent backscattering in nanowire systems.[24] However, for the ballistic regime in our case, these scenarios for the diffusive transport — WL or WAL — could be ruled out. Although the effective g^* factor of InSb nanowires is quite large ($\sim$ 30–50), the Zeeman energy of such low magnetic field (0.5 T) $E_Z = |g^*|\mu_B B \sim 1$ meV is still negligible compared to the spacing of the 1D subbands $\Delta E \sim 15$ meV–25 meV. Thus, the influence from the depopulation of 1D subbands on

the conductance could be also omitted in this case. To clarify, we subtract the varying background at zero magnetic field $G(0)$ from the MC data to get $\Delta G = G(B) - G(0)$. This allows us to focus on the variation of conductance caused by the applied magnetic field. The corresponding result $\Delta G(B, V_g)$ is displayed as a 2D plot in Fig. 3(b). As can be clearly seen, ΔG exhibits periodic-like resonances as B or V_g is changed, which implies close correlation with the Fabry–Pérot interference. We interpret these resonances as the constructive interferences induced by the magnetic field. In the presence of a perpendicular magnetic field, the traveling electrons in the nanowire will accumulate an additional phase $\Delta\varphi$ in their wave functions, leading to a variation of interference conditions with varying magnetic field.

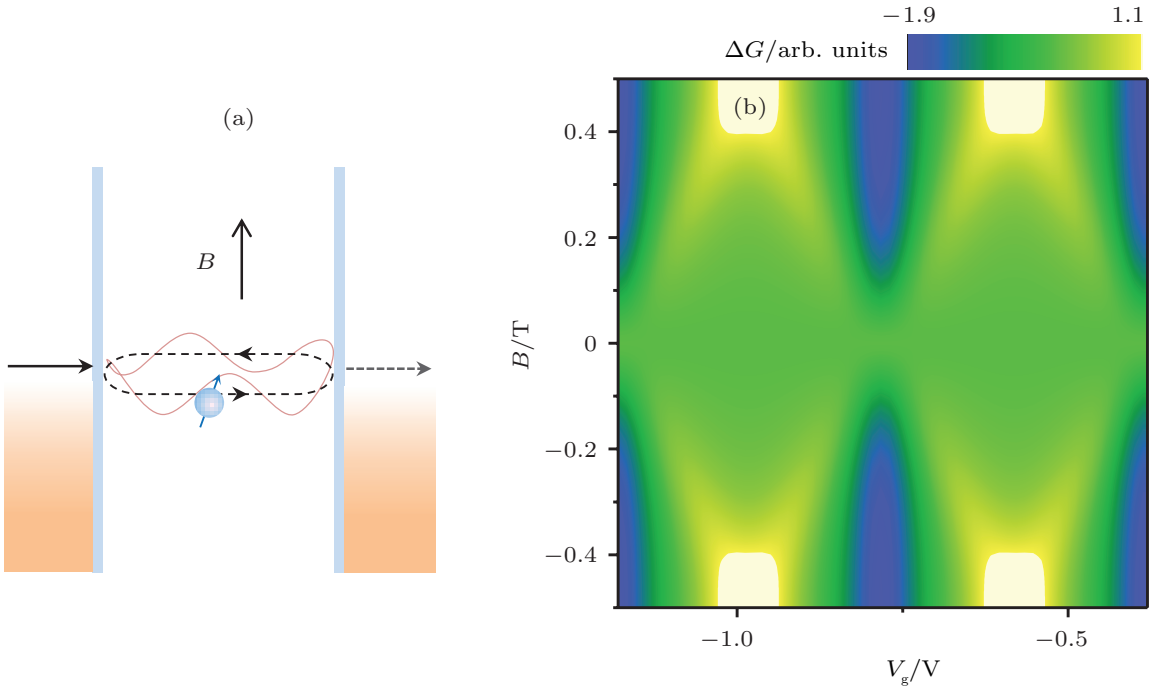


Fig. 4. (color online) (a) Schematic diagram of the transport model of electrons in a ballistic metal–nanowire–metal device under a perpendicular magnetic field. As a result of ballistic regime, electrons get only reflected at the two interfaces. The red curve refers to the electron wave of the interference process. (b) Simulated subtracted magnetoconductance ΔG as a function of the gate voltage and the magnetic field. The results show a good qualitative agreement with the experimental measurements shown in Fig. 3(b).

Based on this scenario, the evolution of gate-tuned magnetoconductance can be understood quantitatively on the basis of a simple model shown schematically in Fig. 4(a). In this picture, the conductance G should be proportional to the probability of electrons propagating into the contact, which can be expressed in terms of the square of the electron's wave function, i.e.,

$$G \propto |\sum_n \alpha^{2n} \mathrm{e}^{\mathrm{i}k(2n+1)L}|^2,$$

where α is the reflective coefficient and n denotes the times of reflection. In a ballistic nanowire device, the application of a magnetic field induces an additional phase shift $\Delta\varphi_j = BS_j/\Phi_0$, where S_j is the area of the j-th trajectory of bouncing electrons and $\Phi_0 = h/2e$ is the flux quanta. Taking this into account, the conductance in the magnetic field becomes

$$G \propto |\sum_{n,j} \alpha^{2n} \mathrm{e}^{\mathrm{i}k(2n+1)L+\Delta\varphi_j}|^2.$$

We use this model to perform simulation of the conductance and the obtained result is shown in Fig. 4(b). It is clear that the main features of the experimental result can be well reproduced by this model, which therefore strongly supports our interpretation.

4. Conclusion

In conclusion, we have demonstrated comprehensive evidences for the ballistic transport in superconductor contacted InSb nanowires devices. We observe clear plateaus of conductance in a nanowire at a temperature of 10 K and zero magnetic field with the ability to accurately control the population of the 1D subbands. At a lower temperature, we have observed characteristic Fabry–Pérot resonances which confirm the ballistic nature of charge transport in the InSb nanowire. We further demonstrate the quantum interferences effects on the conductance of nanowire in the presence of a magnetic field. The magnetoconductance data in the Fabry–Pérot regime can be well explained by considering the phase shift induced by the magnetic field in a ballistic nanowire, which is further verified by our simulation. Given the strong spin-orbit interaction in InSb nanowires, more exotic features of transport, such as the helical modes,[32] deserve attention in such systems in future studies. Our results pave the way towards tailoring the desired

1D topological modes and understanding of coherent transport in superconductor contacted InSb nanowires.

References

[1] Del Alamo J A 2011 *Nature* **479** 317

[2] Nilsson H, Deng M T, Caroff P, Thelander C, Samuelson L, Wernersson L E and Xu H Q 2011 *IEEE J. Sel. Top. Quantum Electron.* **17** 907

[3] Pribiag V, Nadj-Perge S, Frolov S, van den Berg J, van Weperen I, Plissard S, Bakkers E and Kouwenhoven L P 2013 *Nat. Nanotechnol.* **8** 170

[4] Frolov S M, Plissard S R, Nadj-Perge S, Kouwenhoven L P and Bakkers E P A M 2013 *MRS Bulletin* **38** 809

[5] Nadj-Perge S, Pribiag V S, van den Berg J W, Zuo K, Plissard S R, Bakkers E P, Frolov S M and Kouwenhoven L P 2012 *Phys. Rev. Lett.* **108** 166801

[6] van Weperen I, Tarasinski B, Eeltink D, Pribiag V S, Plissard S R, Bakkers E, Kouwenhoven L P and Wimmer M 2015 *Phys. Rev. B* **91** 1413

[7] Stephens A, Seiler D, Sybert J and Mackey H 1975 *Phys. Rev. B* **11** 4999

[8] Nilsson H A, Caroff P, Thelander C, Larsson M, Wagner J B, Wernersson L E, Samuelson L and Xu H Q 2009 *Nano Lett.* **9** 3151

[9] Fan D, Li S, Kang N, Caroff P, Wang L B, Huang Y Q, Deng M T, Yu C L and Xu H Q 2015 *Nanoscale* **7** 14828

[10] Lutchyn R M, Sau J D and Das Sarma S 2010 *Phys. Rev. Lett.* **105** 077001

[11] Oreg Y, Refael G and von Oppen F 2010 *Phys. Rev. Lett.* **105** 177002

[12] Mourik V, Zuo K, Frolov S M, Plissard S R, Bakkers E P A M and Kouwenhoven L P 2012 *Science* **336** 1003

[13] Deng M T, Yu C L, Huang G Y, Larsson M, Caroff P and Xu H Q 2012 *Nano Lett.* **12** 6414

[14] van Wees B J, Kouwenhoven L P, Willems E M M, Harmans C J P M, Mooij J E, van Houten H, Beenakker C W J, Williamson J G and Foxon C T 1991 *Phys. Rev. B* **43** 12431

[15] Wharam D, Thornton T, Newbury R, Pepper M, Ahmed H, Frost J, Hasko D, Peacock D, Ritchie D and Jones G 1988 *J. Phys. C: Solid State Phys.* **21** L209

[16] Liang W J, Bockrath M, Bozovic D, Hafner J H, Tinkham M and Park H 2001 *Nature* **411** 665

[17] Javey A, Guo J, Wang Q, Lundstrom M and Dai H 2003 *Nature* **424** 654

[18] Kretinin A V, Popovitz-Biro R, Mahalu D and Shtrikman H 2010 *Nano Lett.* **10** 3439

[19] Li S, Kang N, Fan D X, Wang L B, Huang Y Q, Caroff P and Xu H Q 2016 *Sci. Rep.* **6** 24822

[20] Heedt S, Prost W, Schubert J, Grützmacher D and Schäpers T 2016 *Nano Lett.* **16** 3116

[21] Kammhuber J, Cassidy M C, Zhang H, Gul O, Pei F, de Moor M W, Nijholt B, Watanabe K, Taniguchi T, Car D, Plissard S R, Bakkers E P and Kouwenhoven L P 2016 *Nano Lett.* **16** 3482

[22] Hansen A, Björk M, Fasth C, Thelander C and Samuelson L 2005 *Phys. Rev. B* **71** 205328

[23] Roulleau P, Choi T, Riedi S, Heinzel T, Shorubalko I, Ihn T and Ensslin K 2010 *Phys. Rev. B* **81** 155449

[24] Wang L B, Guo J K, Kang N, Pan D, Li S, Fan D, Zhao J and Xu H Q 2015 *Appl. Phys. Lett.* **106** 173105

[25] Vigneau F, Prudkovkiy V, Duchemin I, Escoffier W, Caroff P, Niquet Y M, Leturcq R, Goiran M and Raquet B 2014 *Phys. Rev. Lett.* **112** 076801

[26] Holloway G W, Shiri D, Haapamaki C M, Willick K, Watson G, LaPierre R R and Baugh J 2015 *Phys. Rev. B* **91** 045422

[27] Thelander C, Caroff P, Plissard S B and Dick K A 2012 *Appl. Phys. Lett.* **100** 232105

[28] Xu T, Dick K A, Plissard S, Nguyen T H, Makoudi Y, Berthe M, Nys J P, Wallart X, Grandidier B and Caroff P 2012 *Nanotechnology* **23** 095702

[29] Liao G, Luo N, Yang Z, Chen K and Xu H Q 2015 *J. Appl. Phys.* **118** 094308

[30] Chuang S, Gao Q, Kapadia R, Ford A C, Guo J and Javey A 2013 *Nano Lett.* **13** 555

[31] Bagwell P F and Orlando T P 1989 *Phys. Rev. B* **40** 1456

[32] Rainis D and Loss D 2014 *Phys. Rev. B* **90** 235415